Arabian Journal of Chemistry (2020) 13, 7533–7543

King Saud University

Arabian Journal of Chemistry

www.ksu.edu.sa
www.sciencedirect.com

ORIGINAL ARTICLE

Fabrication of $SiO_2/CuFe_2O_4$/polyaniline composite: A highly efficient adsorbent for heavy metals removal from aquatic environment

Md. Abu Taleb [a], Rajeev Kumar [a], Awad A. Al-Rashdi [b], Moaaz K. Seliem [c], M.A. Barakat [a,d,*]

[a] *Department of Environmental Sciences, Faculty of Meteorology, Environment and Arid Land Agriculture, King Abdulaziz University, Jeddah 21589, Saudi Arabia*
[b] *Department of Chemistry, Al-Qunfudhah University College, Umm Al-Qura University, Saudi Arabia*
[c] *Department of Applied Mineralogy, Faculty of Earth Science, Beni-Suef University, 621, Egypt*
[d] *Central Metallurgical R & D Institute, Helwan 11421, Cairo, Egypt*

Received 26 June 2020; accepted 27 August 2020
Available online 3 September 2020

KEYWORDS

$SiO_2/CuFe_2O_4$/polyaniline;
Adsorption;
Bivalent metal ions;
Synthetic wastewater

Abstract A novel multifunctional of $SiO_2/CuFe_2O_4$/polyaniline composite was synthesized through the interaction between silica (SiO_2), copper iron oxide ($CuFe_2O_4$), and polyaniline (PANI) as starting materials. $SiO_2/CuFe_2O_4$/polyaniline composite was characterized for morphology, crystallinity, textural properties, and utilised for the removal of Fe(II), Mn(II), and Cu(II) from synthetic wastewater solutions. The roles of solution pH (2.0–6.0), interaction time (15–420 min), initial ion concentration (50–700 mg/L), and solution temperature (30–50 °C) in the adsorption process were investigated. The adsorption capacities of $SiO_2/CuFe_2O_4$/PANI for the tested metal ions were high compared to SiO_2, $CuFe_2O_4$, and polyaniline. Equilibrium studies indicated that Fe(II) and Mn(II) adsorption were compliant with the Langmuir model, while the Freundlich equation described the removal of Cu(II) ions. The maximum Langmuir capacities were up to 285.71, 416.67, and 454.55 mg/g for Cu(II), Fe(II), and Mn(II), respectively. The pseudo-first-order kinetic model fitted well the metal ions removal data. The rate-controlling step reflected the involvement of surface and inner pore diffusion (intraparticle) processes. Electrostatic attractions and chelation were mainly responsible for the binding of metals ions onto $SiO_2/CuFe_2O_4$/PANI. The selectivity

* Corresponding author at: Department of Environmental Sciences, Faculty of Meteorology, Environment and Arid Land Agriculture, King Abdulaziz University, Jeddah 21589, Saudi Arabia.
E-mail address: mababdullah1@kau.edu.sa (M.A. Barakat).
Peer review under responsibility of King Saud University.

Production and hosting by Elsevier

https://doi.org/10.1016/j.arabjc.2020.08.028

of the studied ions was governed mainly by the hydrated ionic radii and the composite adsorption active sites. $SiO_2/CuFe_2O_4$/PANI can be easily reused with a slight decrease (around 2–3%) in metal removal efficiency after four successive regeneration cycles.

1. Introduction

In recent times, the pollution of water bodies due to the continuous discharge of contaminated chemicals as heavy metals is considered as one of the serious environmental problems (Feng et al., 2020). Metallic contaminants are discharged into aquatic surroundings from natural sources (dissolving rocks) and industrial processes, including landfilling, pesticide production, oil processing, and mining (Irshad et al., 2020). Long-term, amassing metal ions in the living body leads to health and economic problems due to the biological toxicity of these polluted ions (Shao et al., 2020; Irshad et al., 2020; Jin et al., 2019). Heavy metals, including iron (Fe^{2+}), manganese (Mn^{2+}), and copper (Cu^{2+}), are common in the lithosphere (Awual et al., 2015). The pollution of water by Fe(II)-/Mn(II) ions produces poor water taste, colour, odour, and turbidity; Fe(II)-/Mn(II) water pollution also causes various chronic diseases (Aziz et al., 2020; Dou et al., 2018; Du et al., 2017). Further, while low concentrations of Cu^{2+} are required for human health, high concentrations are toxic and carcinogenic (Gupta et al., 2020).

Approaches for effective sequestration of metal ions from water include ion-exchanger resins, membrane filtration, precipitation, and adsorption (Patil et al., 2016; Youssef et al., 2019; Seliem and Komarneni, 2016; Barakat et al., 2019). Adsorption is considered as a simple, environmentally friendly, and cost-effective method for the removal of different water contaminates as compared to the other techniques (Wei et al., 2018; Malik et al., 2017; Shao et al., 2019; Cai et al., 2020). Substances used to remove metal ions from polluted water via adsorption include activated carbon, silica, alumina, graphene oxide, polyaniline, nanosized ferric oxides, manganese oxides, and titanium oxides (Renu et al., 2017).

Recently, scientists have focused on the fabrication of new multifunctional adsorbents for their low costs and simple utilization. Nanoparticles precursors may prove to be valuable as adsorbents due to their unique characteristics, including small size, available reactive sites, and high efficiency of regeneration (Ordinartsev et al., 2018; Kumar et al., 2019; Daka et al., 2020). In addition, metal nanoparticles have distinct optical, mechanical, catalytic, and electrochemical properties and thus, they have well-recognized in different applications including water remediation (Ge et al., 2020). Another approach is the rapid removal of water contaminates through magnetic separation because of its simplicity and high efficiency (Zhang et al., 2007).

Ferrites or metal iron oxide nanoparticles are considered to be stable chemical compounds with unique magnetic, optical, and electrical properties (Hussain et al., 2020). Consequently, these compounds are used in the biomedical, environmental science, and electronics industries (Yousuf et al., 2020). Copper–iron spinels ($CuFe_2O_4$) are cubic, close–packed arrangements of oxygen ions that include Cu^{2+} and Fe^{3+} ions at two distinct crystallographic sites (Sun et al., 2020; Zhang et al., 2020). $CuFe_2O_4$ nanoparticles are used in heterogeneous catalysis, energy storage, drug delivery, and magnetic separation (Sun et al., 2020). In aquatic systems, however, the aggregation of iron oxides into large clusters causes ferrites to lose their adsorbent properties, especially for inorganic contaminates (Fotukian et al., 2020).

Silica (SiO_2), when linked to the surface of magnetic nanoparticles, prevented the aggregation of iron oxide nanoparticles in water (Barik et al., 2020; Renu et al., 2017). The interaction between silanol groups of silica and the magnetic nanoparticle's surface resulted in the formation of composites with various functional groups (Barik et al., 2020; Wei et al., 2018).

Polyaniline (PANI), a distinctive conjugated polymer, has attracted further consideration because of its ease of preparation, low price, and environmental stability (Dinari and Neamati, 2020; Cabuk et al., 2014). Furthermore, synthetic PANI composites have multifunctional groups (active sites) and show high adsorption capacities for organic and inorganic contaminants (Stejskal 2020; Deng et al., 2020a,b; Lai et al., 2014). Fabrication of $SiO_2/CuFe_2O_4$/polyaniline composite as a hybrid ternary adsorbent is significant to increase of functional groups (adsorption active sites) and consequently increase the removal efficiency of the inorganic metal ions from solutions. Also, the fabricated hybrid ternary composite provides the maximum adsorption capacitance and, therefore, the addition of other materials, such as silica, to $CuFe_2O_4$ nanoparticles can enhance the adsorption properties of magnetic nanoparticles in aquatic environments.

The purpose of this study was to prepare, characterise, and test a new $SiO_2/CuFe_2O_4$/PANI composite for Fe(II), Mn(II), and Cu(II) ions scavenging. The roles of different experimental parameters in controlling the adsorption capability of $SiO_2/CuFe_2O_4$/PANI against Fe(II), Mn(II), and Cu(II) ions were evaluated. Moreover, equilibrium and kinetic parameters were determined to ascertain the adsorption mechanism of the metals ions onto the fabricated composite.

2. Materials and methods

2.1. Materials

Heavy metals were used which included ferrous sulphate ($FeSO_4{\cdot}7H_2O$), manganese chlorite ($MnCl_2{\cdot}4H_2O$), and copper sulphate ($CuSO_4.5\ H_2O$) (BHD Chemical, Poole, England). Tetraethyl orthosilicate (TEOS, purity 97%), and sodium lauryl sulfate (SLS) were received from Scharlab S. L., Spain. HCl, NaOH, and ethanol were used as pure grades in this work. Polyaniline was chemically prepared using aniline (Sigma-Aldrich Co., USA) and ammonium persulphate ($(NH_4)_2S_2O_8$ (BHD Chemical, Poole, England). The HACH perachem reagents (HACH LANGE Gmbh, Ger-

many), ferrous iron reagents (cat. 1037690), sodium periodate (cat 2107769) and CuVer 1 copper reagent (cat 2105869) were used for the analysis of Fe(II), Mn(II) and Cu(II), respectively.

2.2. Synthesis of adsorbents

The adsorbents (SiO_2, $CuFe_2O_4$, and $SiO_2/CuFe_2O_4$/PANI composite) were prepared as follows.

2.2.1. Synthesis of SiO_2

First, 1.3 g of sodium lauryl sulfate (SDS) was dissolved in 25 mL of deionised water. Next, 3.5 mL of tetraethyl orthosilicate (TEOS) was mixed with 25 mL ethanol solution and poured to the SDS mixture. While constantly stirring for 30 min, 12 mL of NH_4OH was added dropwise. After stirring for 60 min, the white precipitate was transferred to a hydrothermal reactor and treated at 140 °C for 24 h. The produced silica was washed several times and dehydrated at 105 °C/ 24 h.

2.2.2. Synthesis of $CuFe_2O_4$

Copper ferrites ($CuFe_2O_4$) were synthesized by mixing 1.997 g of copper sulphate ($CuSO_4{\cdot}5H_2O$) and 7.791 g of ferrous sulphate ($FeSO_4{\cdot}7H_2O$) with 80 mL deionised water. The pH of the solution was increased to 11 by using 0.1 M NaOH. Next, 150 mL of the solution was transferred to a hydrothermal reactor before treatment at 150 °C for 18 h. Finally, the precipitate $CuFe_2O_4$ was washed and dried at 100 °C for 24 h.

2.2.3. Synthesis of the composite $SiO_2/CuFe_2O_4$/PANI

First, 1.3 g SDS was added to 25 mL distilled water and mixed with 25 mL of ethanol containing 1.5 mL of TEOS. Next, 0.8 g of $CuFe_2O_4$ and 3 mL of aniline (99.5%) solution was added and mixed under continuous stirring. Finally, 6 mL of NH_4OH (25%) was added dropwise. The solution was transferred to the hydrothermal reactor for treatment at 140 °C for 24 h. The $SiO_2/CuFe_2O_4$/PANI was centrifuged and washed multiple times using deionised water and acetone. The resultant solid was dried at 50 °C for 24 h and homogenised.

2.3. Characterisation of the adsorbents

X–ray diffraction was used to analyse $CuFe_2O_4$, SiO_2, and $SiO_2/CuFe_2O_4$/PANI (Pananalytical X'Pert PRO 3040/60, Netherlands). X–ray photoelectron spectroscopy (XPS) was used to analyse the $SiO_2/CuFe_2O_4$/PANI composite (SPECS spectrometer, GmbH, Germany). The morphological features of the as–synthesized products were recorded (JEOL, Tokyo, Japan and FEI Techni, G2 F20, USA with 1.0 kV and 200 kV acceleration voltage, respectively). The BET-surface area, pore volume, and pore size of SiO_2 and $SiO_2/CuFe_2O_4$/PANI composite were determined using (Quantachrome Autosorb-1 surface area analyser, USA).

2.4. Fe(II), Mn(II), and Cu(II) scavenging studies

Three stock solutions of the investigated bivalent metals were separately prepared by mixing proper amounts of ferrous sulphate ($FeSO_4{\cdot}7H_2O$), manganese chlorite ($MnCl_2{\cdot}4H_2O$), and copper sulphate ($CuSO_4{\cdot}5H_2O$) in 1 L of deionised water each. Subsequently, distilled water was mixed with the prepared stock solutions (1 g/L) to obtain the needed initial concentrations of the adsorption experiments. The next step was to explore the influence of experimental parameters on the scavenging of metal ions. A series of adsorption tests using 0.02 g of the adsorbent was conducted in the single metal solution. All pH, ions concentrations, shaking time experiments were carried out at 30 °C. Adsorption tests were repeated three times; the average values are reported. After equilibrium attainment, the samples were filtered using a 0.45 μm PTFE syringe membrane while for the regeneration study, the adsorbents was separated by centrifuge from the solution. The remaining concentrations of metal ions were determined using specific HACH kits on a DR–6000 UV–visible spectrophotometer within the ranges of (1μg/L to 8.0 mg/L), (0.02 mg/L to 3.0 mg/L), and (0.006 mg/L to 20.0 mg/L) for Cu(II), Fe(II) , and Mn(II), respectively.

The role of solution pH was examined at pHs between 2.0 and 6.0 to avoid the precipitation of metal ions at higher pH values.

- Different initial concentrations of metal ions (ranging from 50 to 700 mg/L) were used to find the influence of the starting concentration.
- The effect of contact time was examined from 15 to 420 min.
- The effect of temperature was assessed at 30, 40, and 50 ^{o}C using 20 mL of 500 mg/L of each ion concentration.

The scavenging percentage (R %) of the studied ions, the removed amounts at adsorption equilibrium (q_e), and quantity of metal adsorbed at time (q_t) were determined according to the following equations:

$$\mathrm{R}\ (\%) = \frac{(\mathrm{C0} - \mathrm{Ct})}{\mathrm{C0}} \times \tag{1}$$

$$q_e(\mathrm{mg/g}) = (C_0 - C_e)\frac{V}{m} \tag{2}$$

$$q_t(\mathrm{mg/g}) = (C_0 - C_t)\frac{V}{m} \tag{3}$$

Where, C_t, C_0, and C_e are the metal concentration at the initial time and the equilibrium (mg/L), respectively. V is the volume (L) of the metal ion solutions, and m is the adsorbent mass (g).

2.5. Surface charge analysis

The point of zero charge (pH_{PZC}) value is necessary to evaluate the adsorbent surface charge. In this study, 0.1 M KCl solution and adsorbent mass (0.02 g) of SiO_2 and $SiO_2/CuFe_2O_4$/PANI were used to determine the pH_{PZC} values. The adsorbent dose was transferred to 20 mL solutions of the pH ranging 2–9. The solutions were mixed in an agitated water bath for 24 h at 30 ^{0}C. The final pH of each solution was determined. A graph between the beginning and final pH was plotted to obtain the pH_{PZC} of the SiO_2 and $SiO_2/CuFe_2O_4$/PANI.

3. Results and discussion

3.1. Materials characterisation

The morphological characteristics of SiO_2 and $SiO_2/CuFe_2O_4$/PANI are displayed in Fig. 1. SEM images of silica particles show agglomerated particles with spherical shapes (Fig. 1a). SEM of the fabricated $SiO_2/CuFe_2O_4$/PANI (Fig. 1b) exhibited compacted and agglomerated particles with different shapes in contact with the spherical SiO_2 particles. The SEM image for the $CuFe_2O_4$ is shown in Fig. S1. The morphological analysis of the $CuFe_2O_4$ showing the cubical shape particle of the different size. The presence of grains with a cubic shape of $CuFe_2O_4$ as well as distributed, clustered, thin particles of PANI confirmed the successful preparation of the adsorbents.

TEM images of SiO_2 (Fig. 2a) revealed that the spherical porous SiO_2 particles were strongly agglomerated. On the other hand, Fig. 2b and 2c displayed the existence of cubic and semi-spherical shape particles. The cubic shape was associated with $CuFe_2O_4$; the spherical particles with porous structure could be related to $SiO_2/CuFe_2O_4$/PANI interaction. Several findings support the successful fabrication of the $SiO_2/CuFe_2O_4$/PANI composite: the existence of the agglomerated cubic nanoparticles with a diameter of less than 100 nm of $CuFe_2O_4$; the clustered thin layer of PANI; and the spherical-like SiO_2 particles (Fig. 2).

The textural characteristics of SiO_2 and $SiO_2/CuFe_2O_4$/PANI composite are studied using BET analysis and are tabulated in Table S1. The specific surface areas, average pore size, and total pores volume were observed to be 225 m^2/g, 9.08 nm, and 0.012 cm^3/g for SiO_2, while 75.21 m^2/g, 9.16 nm and 0.00344 cm^3/g, for $SiO_2/CuFe_2O_4$/PANI composites, respectively. The decrease of both surface area and pore volume of the $SiO_2/CuFe_2O_4$/PANI composite as compared to SiO_2 could be attributed to the interaction with PANI (Tang et al., 2014). This interaction blocked the pores of SiO_2 particles, decreasing the $SiO_2/CuFe_2O_4$/PANI surface area. Also, the SiO_2 average pore size was low compared to the $SiO_2/CuFe_2O_4$/PANI composite (Tang et al., 2014).

Fig. 3 displays the XRD patterns of the fabricated SiO_2, $CuFe_2O_4$, and $SiO_2/CuFe_2O_4$/PANI. The XRD pattern of SiO_2 exhibits the occurrence of one strong reflection peak at $2\theta = 22°$ (200), which is in the form of amorphous tridymite matching with JCPD card (01–073-6614). The XRD patterns of $CuFe_2O_4$ reflect the presence of iron oxide, and copper iron oxide, which match the JCPD cards of 01–084-0308, 00–034-0425, 00–006-0545, and 00–003-0870, respectively. These identified minerals were detected at $2\theta = 33.29°$, 35.87°, 49.64°, 54.17°, and 62.54° (Fig. 3). Moreover, the XRD pattern of $SiO_2/CuFe_2O_4$/PANI composite displays the presence of similar peaks for iron oxide, and copper iron oxide with the slight shift in the peak position ($2\theta = 33°$, 35.90°, and 62.13°) and peak intensity. However, the peaks for PANI and SiO_2 were not observed in the XRD pattern of $SiO_2/CuFe_2O_4$/PANI composite due to the small amount of the PANI and the good interaction between silica particles and the $CuFe_2O_4$/PANI of this composite. The XRD pattern of transition metal based materials start with higher intensities and give elevated trajectory towards higher 2θ (Shimano and Mac Diarmid, 2001; Mujasambatoo, et al., 2011).

The XPS analysis of the synthesized $SiO_2/CuFe_2O_4$/PANI composite is illustrated in Fig. 4. The elements identified were Si, O, Cu, Fe, C and N related to SiO_2, $CuFe_2O_4$, and PANI in $SiO_2/CuFe_2O_4$/PANI composite. The wide scan survey of $SiO_2/CuFe_2O_4$/PANI composite (Fig. 4a) shows the peaks at the binding energies of 103.66 eV (Si 2p), 284.91 eV (C1s), 399.56 eV (N 1 s), 532.86 eV (O1s), 710.16 eV(Fe 2p), and 933.46 eV (Cu 2p).

The deconvoluted XPS spectrum of C 1 s displayed five different peaks at 283.5, 284.8, 285.68, 286.77, and 298.69 eV (Fig. 4b). These peaks correspond to C/C = C, C/C-C/C-H, C-O/C-NH, and absorbed CO_2 as C = O and O-C = C groups of PANI in the $SiO_2/CuFe_2O_4$/PANI composite.

The Si 2p shows another two peaks of 102.61 eV for Si–O–Si and 103.73 for SiO_2 (Fig. 4e). Moreover, the O 1 s deconvoluted XPS spectrum peaks at 530.37, 532.75, and 533.43 eV represent the lattice O and surface –OH groups of SiO_2 and $CuFe_2O_4$ in $SiO_2/CuFe_2O_4$/PANI (Fig. 4c).

On the other hand, N 1 s had two peaks (398.69 for N=/C = N-C and 399.67 for N-H-/pyridinic N (Fig. 4d) due to its different electronic states. Fe $2p_{3/2}$ also shows peaks at 710.34 and 712.79 (Fig. 4f). Cu $2p_{3/2}$ appears at 933.36 eV for Cu-O (Fig. 4g) in $CuFe_2O_4$.

3.2. Effect of pH

Low pH is suitable for the protonation of the adsorbent surface, while increased pH results in the domination of the

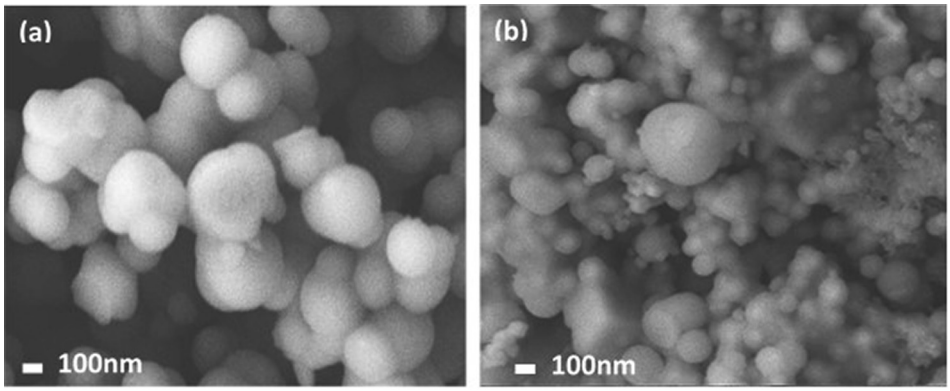

Fig. 1 SEM of (a) SiO_2, and (b) $SiO_2/CuFe_2O_4$/PANI composite.

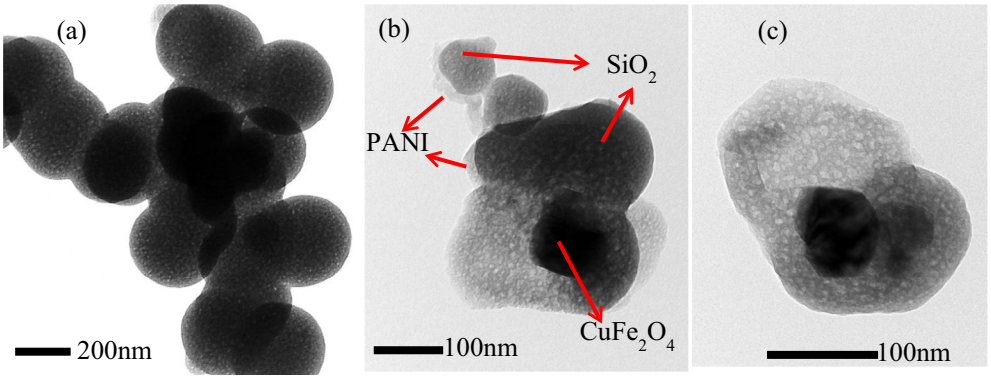

Fig. 2 TEM of (a) SiO_2 and (b, c) $SiO_2/CuFe_2O_4$/PANI composite.

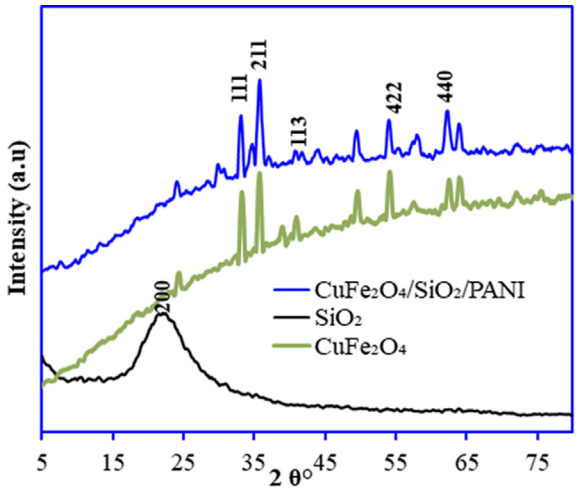

Fig. 3 X-ray diffraction patterns of SiO_2, $CuFe_2O_4$ and $SiO_2/CuFe_2O_4$/PANI composite.

deprotonated sites (Siyal et al., 2018). The variation in the pH of a metal ion solution, therefore, plays a significant role in the adsorption system. The next step was to identify the influence of solution pH on the adsorption of Fe(II), Mn(II) and Cu(II). Thus, 0.02 g of SiO_2, $CuFe_2O_4$, PANI, and $SiO_2/CuFe_2O_4$/PANI were mixed with 500 mg/L of initial metal concentrations for five h at 30 °C within pH ranging from 2.0 to 6.0. For all adsorbents, the adsorbed amounts of the tested metal ions increased with rising pH (Fig. 5). This behaviour can be explained on the basis of point of zero change (pH_{zpc}) of the adsorbent. The pH_{zpc} of SiO_2 and $SiO_2/CuFe_2O_4$/PANI were found at a pH of approximately 4.0 and 5.0, respectively (Fig. S2 in supplementary data). The decrease of metal ions removal at low pH could be related to the existence of high quantities of H^+, which compete with Fe(II), Mn(II) and Cu (II) for the adsorbents active sites (Seliem and Komarneni, 2016). The high removal percentages at high pH values could be associated with the electrostatic interaction between the positive metal ions and negative surface charges of the adsorbents. Compared to all adsorbents, the $SiO_2/CuFe_2O_4$/PANI

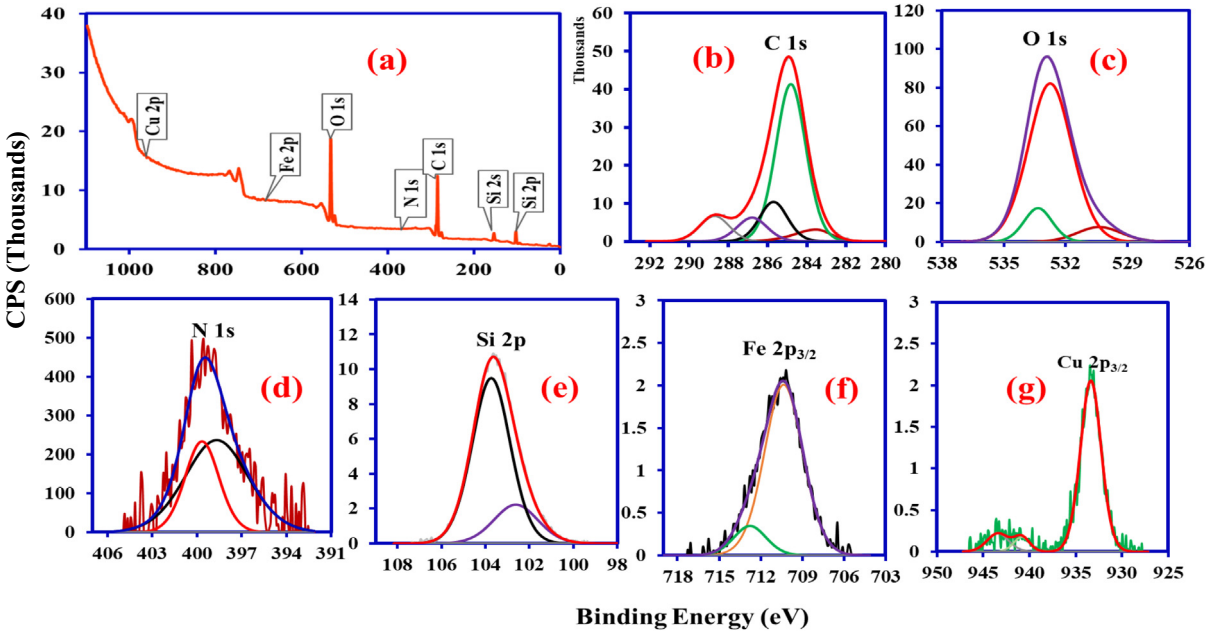

Fig. 4 XPS spectra of $SiO_2/CuFe_2O_4$/PANI composite (a) scan survey (b) C 1 s (c) O 1 s (d) N 1 s (e) Si 2p (f) Fe $2p_{3/2}$ (g) Cu $2p_{3/2}$.

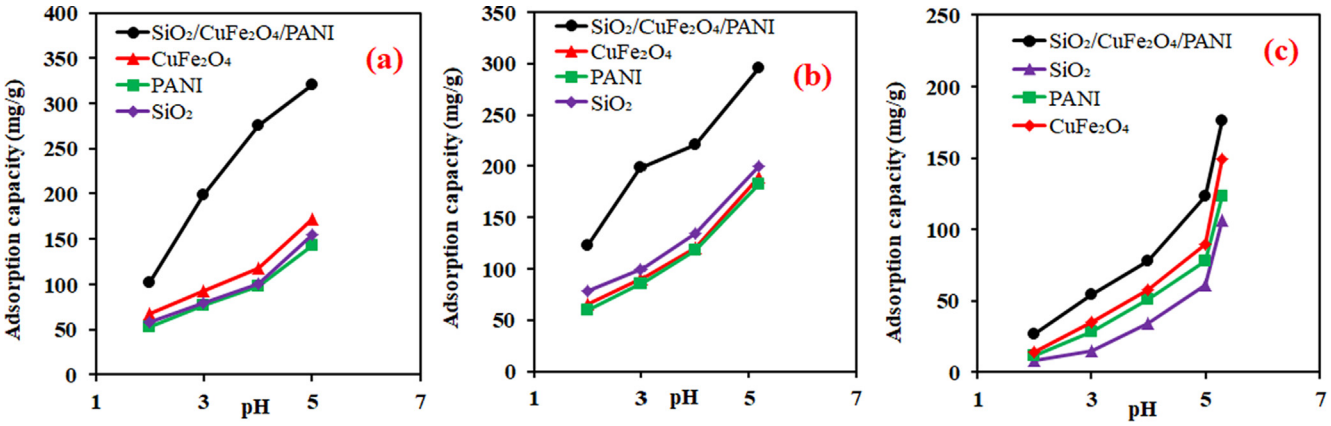

Fig. 5 Effect of pH on the adsorption of metal ions onto the different adsorbents; (a) Fe(II), (b) Mn(II), (c) Cu(II). (metal concentration (500 mg/L), time (5 h), temperature (30 °C), volume (20 mL), adsorbent mass (0.02 g.)

composite displayed the highest values for Fe(II), Mn(II), and Cu(II) scavenging due to its functionality and bulk active sites. These results revealed that existence of SiO_2, $CuFe_2O_4$, and PANI in the composite play a synergetic effect to enhance the adsorption capacity compared to the pure one. Therefore, it can conclude that chelation of the studied metals with anionic active sites and electrostatic attraction are the main parameters that resulted in the improving removal efficiency of the composite (Yadav et al., 2019).

The pH study revealed that optimum removal of Fe(II), Mn(II), and Cu(II) was observed at pH 5.0, 5.18, and 5.3, respectively. Based on the pH experiment, the effect of other parameters was performed only for the $SiO_2/CuFe_2O_4$/PANI composite at pH = 5.0.

3.3. Metal ions concentration effect

The scavenging of Fe(II), Mn(II), and Cu(II) onto $SiO_2/CuFe_2O_4$/PANI was assessed in metal concentrations ranging from 50 to 700 mg/L (Fig. 6a). The adsorption capacities were enhanced with increasing the initial metal ion concentrations from 50 to 500 mg/L and reached a plateau (i.e., the saturation state) beyond a metal ion concentration of 500 mg/L. The adsorption capacity of $SiO_2/CuFe_2O_4$/PANI for Fe(II), Mn(II), and Cu(II) was increased from 40.5 to 329.8 mg/g, 35.9 to 307 mg/g, and 27.5 to 179.9 mg/L, respectively. The rise in the adsorption capacity with the increase in metal loading capacities was due to the greater driving force by the pressure gradient. While at the saturation point, available vacant sites of $SiO_2/CuFe_2O_4$/PANI occupied with metal ions and equilibrium was attained (Almoisheer et al., 2019).

3.4. Role of contact time

The role of interaction time (15–420 min) is displayed in Fig. 6b. Metal ion removal sharply increased from 15 to 120 min. This finding may be ascribed to the better affinity between the targeted metals ions and the $SiO_2/CuFe_2O_4$/PANI free active sites. Subsequently, the removal capacity of metal ions gradually rose with increased time up to 300 min; this reflects the transfer of iron, manganese, and copper ions from the surface layer to the inner structure of the $SiO_2/CuFe_2O_4$/

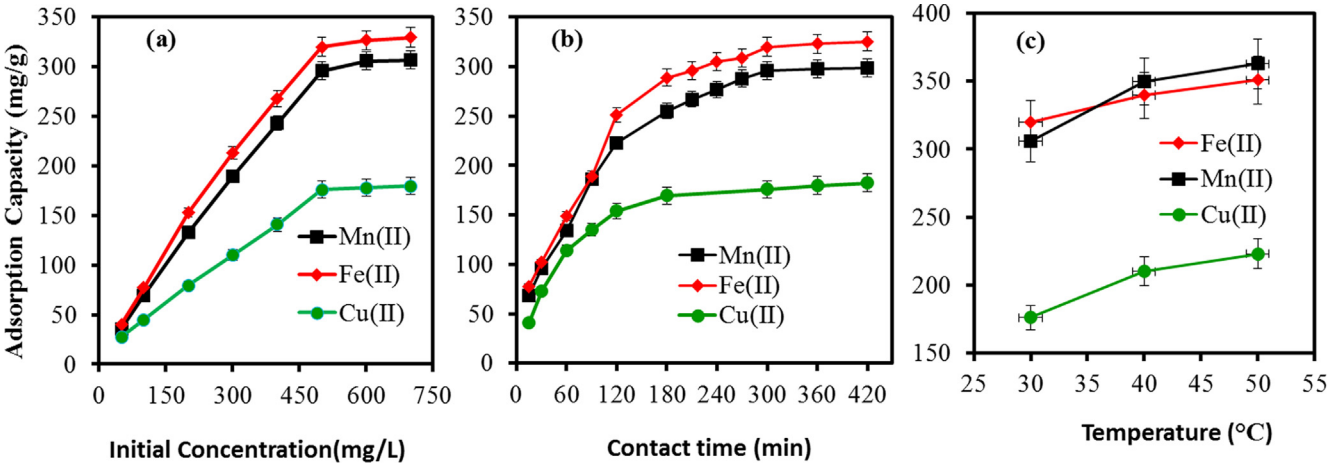

Fig. 6 Adsorption studies on Fe(II), Mn(II) and Cu(II) onto $SiO_2/CuFe_2O_4$/PANI composite; (a) Effect of concentration; (b) Effect of contact time; (c) Effect of temperature; (metal concentration 500 mg/L, pH 5 for Fe(II), pH 5.18 for Mn(II) and pH 5.3 for Cu(II), time 5 hrs, temp 30 °C, adsorbent 0.02 g, volume 20 mL).

PANI (Da'na and Sayari 2013). Next, the metal ion adsorption onto $SiO_2/CuFe_2O_4$/PANI was constant due to reaching equilibrium. Ultimately, 300 min (5 h) of contact time was selected for subsequent studies of this adsorption process.

3.5. Role of solution temperature

The scavenging of Fe(II), Mn(II), and Cu(II) onto $SiO_2/CuFe_2O_4$/PANI was investigated at 30, 40 and 50 °C. The adsorption data (Fig. 6c) indicated that the scavenging of the metal ions was highly related to interaction temperature. Higher solution temperatures enhanced adsorption capacities for Fe(II), Mn(II), and Cu(II) ions. This behaviour reflected the endothermic interactions between the removed ions and the $SiO_2/CuFe_2O_4$/PANI active sites. Thus, diffusion rates of Fe(II), Mn(II), and Cu(II) onto the $SiO_2/CuFe_2O_4$/PANI composite surface increased at higher temperatures (Barakat et al., 2019).

3.6. Isotherms study

To better understand the mechanisms of metal ions adsorption onto the $SiO_2/CuFe_2O_4$/PANI composite, conventional Langmuir and Freundlich models were fitted to the equilibrium data. The Langmuir isotherm model assumes that the formation of a monolayer of adsorbates on a homogenous adsorbent surface has a fixed number of reactive vacancies. Freundlich's model assumes that the various active sites on adsorbent form multilayers of removed ions. The equations for applied models are:

$$\frac{C_e}{q_e} = \frac{1}{q_{\max} b} + \frac{C_e}{q_{\max}} (\text{Langmuir}) \quad (4)$$

$$\log q_e = \log K_F + \frac{1}{n} \log C_e (\text{Freundlich}) \quad (5)$$

Where: $K_F$and b are equilibrium constants (L/g); n and $q_{\max}$ are the strength factor and maximum adsorption capacity (mg/g); and *Ce* is the Fe(II), Mn(II), and Cu(II) equilibrium concentration (mg/L).

Results are presented in Fig. S3 in supplementary data (a, b) and acquired isotherm data were tabulated in Table 1. The Langmuir removal capacities were 416.67, 454.55, and 285.71 mg/g for Fe(II), Mn(II), and Cu(II). These $q_{\max}$values revealed that the active sites on the $SiO_2/CuFe_2O_4$/PANI sites were preferred by the Fe(II) and Mn(II) compared to the Cu (II) ions. This variation could be associated with physicochemical parameters such as ionic radius, hydrated ionic radii, electronegativity, and the adsorbent functional groups (Mobasherpour et al., 2012).

After rendering the R^2 values, the Langmuir model fits the scavenging of Fe(II) and Mn(II), while the Freundlich model fits the removal data of Cu(II). The validity of the Freundlich model for copper ions could be due to variation in the binding sites that removal Cu(II). Fe(II) and Mn(II) ion adsorption, however, occurred through specific and highly selective active sites, which resulted in monolayer coverage. The calculated *n* value for the studied metal ions were 2 less than $10< n$, presented good adsorption characteristics (Kumar et al., 2013; Chen et al., 2015).

3.7. Kinetics studies

The next step was to evaluate the removal rate and explain the adsorption capacity of the adsorbent surface. The adsorption kinetics were investigated by fitting pseudo-first-order (Zhang et al., 2014) and pseudo-second-order kinetic model (Ho and McKay 1999), equations:

$$\log q_e/q_t = \log q_e - k_1 t/2.303 \quad \text{Pseudo} - \text{first} - \text{order} \quad (6)$$

$$t/q_t = (1/k_2 q_e^2) + t/q_t \quad \text{Pseudo} - \text{second} - \text{order} \quad (7)$$

The values of the pseudo-first-order rate constant, k_1 (min^{-1}), and pseudo-second-order rate constant, k_2 (g/(mg. min), were extracted from Fig. S4 in supplementary data.

The calculated values were summarised in Table 2. For Fe (II), Mn(II), and Cu(II), respectively, the R^2 values were: 0.9925, 0.9767, and 0.9954 for the pseudo–first-order; and 0.991, 0.9937, and 0.9557 for the pseudo-second-order. Based on the R^2 values, the applied kinetic models ($R^2 > 0.95$) fit the adsorption processes of the three metals. Moreover, the experimental q_e and the calculated q_e acquired from the pseudo-first-order plot were similar, which supported the suitability of this kinetic model in describing the adsorption of Fe (II), Mn(II), and Cu(II).

The rate of adsorption for all three metal ions can be elucidated by applying these kinetic models. To determine the metal ion diffusion mechanism, however, the intraparticle diffusion model was used:

$$q_t = k_p t^{1/2} + C \quad \text{Intra} - \text{particle diffusion} \quad (8)$$

The plot of q_t versus$t^{1/2}$ was used to obtain the value of the intra-particle diffusion constant k_p(mg/g min), as shown in Fig. 7. The diffusion plots in Fig. 7 for adsorption exhibited three steps with correlation coefficient values > 0.95; these results support the applicability of this model for the three metals. The first step showed the accumulation of metal ions onto the exterior surface of the composite until the outer surface/pores are saturated completely. Next, metal ions diffused into the pores of the composite at a lower diffusion rate in the second step. The third step (the slowest adsorption process) reflected the equilibrium state of the adsorbed Fe(II), Mn (II), and Cu(II) ions onto the composite (Seliem and Komarneni, 2016; Tang et al., 2020). Fig. 7 showing adsorp-

Table 1 Isotherm parameters for the scavenging of metal ions by $SiO_2/CuFe_2O_4$/PANI composite.

Metal	Langmuir isotherm			Freundlich isotherm		
	$q_{m\ (cal)}$ (mg/g)	k_L (mg/L)	R^2	K_F (mg/L)	*n*	R^2
Fe(II)	416.67	4.812	0.9865	0.0412	4.49	0.9482
Mn(II)	454.55	7.416	0.9683	0.0771	5.97	0.9645
Cu(II)	285.71	3.256	0.9444	1.256	5.32	0.9852

Table 2 Kinetics parameters for scavenging of the metal ions by $SiO_2/CuFe_2O_4$/PANI composite.

Metal	Pseudo-first-order				Pseudo-second-order		
	q_e (Exp.)	q_e (mg/g) (cal.)	k_1 (1/min.)	R^2	q_e (mg/g)	k_2 (g/mg. min.)	R^2
Fe(II)	320	333.27	0.01267	0.9925	400	0.0000312	0.991
Mn(II)	296	312.90	0.01221	0.9767	370.37	0.0000330	0.9937
Cu(II)	176	185.18	0.018193	0.9954	185.2	0.000106	0.9557

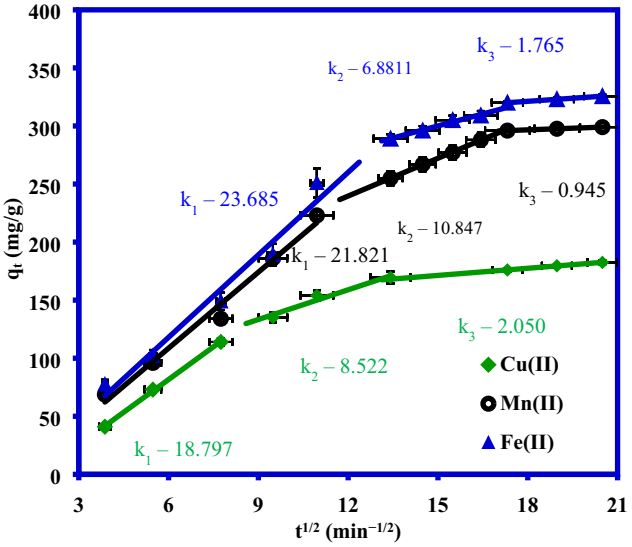

Fig. 7 Plot for the intra–particle diffusion mechanism for Fe(II), Mn(II) and Cu(II) adsorption onto $SiO_2/CuFe_2O_4$/PANI composite.

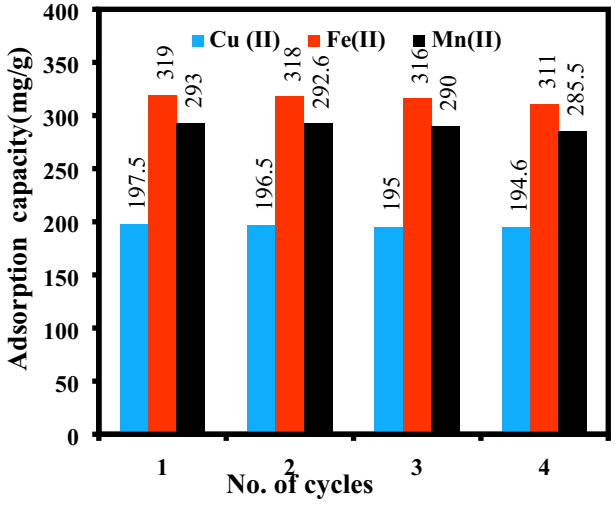

Fig. 8 Desorption studies of Fe(II), Mn(II) and Cu(II) (0.01 M HCl, metal concentration 500 mg/L, pH 5 for Fe(II), pH 5.18 for Mn(II) and pH 5.3 for Cu(II), time (5 h), temperature (30 °C), adsorbent mass (0.02 g), volume (20 mL).

tion of metal ions onto $SiO_2/CuFe_2O_4$/PANI composite was control by both film diffusion and intra-particle diffusion mechanism.

3.8. Regeneration study

The reusability of the synthesized composite was investigated using the eluting agent, 0.1 M HCl. Fig. 8 exhibits the regeneration capacity of Fe(II), Mn(II), and Cu(II) over four successive adsorption–desorption cycles. Adsorption capacities of metal ions by $SiO_2/CuFe_2O_4$/PANI negligibly decreased with increasing cycle number. This finding may be ascribed to the active functional groups and sites on the surface of $SiO_2/CuFe_2O_4$/PANI composite for sequestration of the investigated metal ions. The slight decrease in metal ions removal capacities after each cycle could be mainly related to the irreversible blockage of some active adsorption sites of the adsorbent and then, metal ions are not removed during the regeneration process. Therefore, this adsorbent was simply restored and could be recurrently used for further decontamination of water.

3.9. Adsorption selectivity

The $SiO_2/CuFe_2O_4$/PANI composite showed low selectivity for Cu(II) compared to the Fe(II) and Mn(II). The Cu(II) ionic radii (0.73 Å) is smaller than that of Fe(II) (0.77 Å) and Mn (II) (0.80 Å). Moreover, electronegativity in Cu^{2+} is high (1.9) as compared to that of Fe^{2+} (1.83) and Mn^{2+} (1.55) metal ions. According to the sequences of ionic radii and the values of electronegativity, Cu(II) ions are supposed to show higher adsorption compared to Fe(II) and Mn(II) ions. The observed opposite trend between the ionic radii of the studied metal ions and the adsorption capacities may be associated with the hydration energy (ΔH_{hyd}) of the studied metal ions (Ouyang et al., 2019, Huang et al., 2020, Zhao et al., 2020). The hydration energies of Fe(II), Mn(II), and Cu(II) are – 1950, –1851, and – 2119.3 kJ/mole, respectively (Smith 1977). In the aqueous solution, Cu(II) becomes more hydrolysed due to its high hydration enthalpy and thus, copper ions remain hydrated during the adsorption process. On the other hand, Mn(II) and Fe(II) dehydrate quickly, which increased their adsorption capacities. Consequently, the selectivity performance of the current study confirmed the corresponding relation between the uptake capacity and the hydrolysis properties of the tested heavy metal ions. However, further studies such as statistical physics models are needed to study the selectivity of Cu (II), Mn(II), and Fe(II) in binary and ternary adsorption systems.

3.10. Comparison with other previous studies

Table 3 summarised the maximum scavenging efficiencies of Fe(II), Mn(II), and Cu(II) by different adsorbents. Silica-based polymeric composite adsorbents presented high values due to their high porosity, pore geometry, enlarged surface

Table 3 Comparison of monolayer removal capacities of Fe (II), Mn(II), and Cu(II) by different adsorbents as compared to the $SiO_2/CuFe_2O_4$/PANI composite.

Adsorbents	q_m (mg/g)	References
Fe(II) adsorption		
Coconut shells activated carbon	81.89	Moreno et al., 2011
Chitosan	57.5	Ngah et al., 2005
Chitosan/polyethylene glycol membrane	90.9	Reiad et al., 2012
Cross-linked chitosan	64.1	Moreno et al., 2011
$SiO_2/CuFe_2O_4$/PANI	416.67	this study
Mn(II) adsorption		
Fe_2O_3/SiO_2/PAN	126.16	Ramutshatsha et al., 2019
Coconut shells Activated carbon	75.65	Moreno et al., 2011
Polyvinyl alcohol/ β-cyclodextrin	90.28	Zhang et al., 2019
Alginate-combusted coal gangue	64.29	Mohammadi et al., 2019
$SiO_2/CuFe_2O_4$/PANI	454.55	this study
Cu(II) adsorption		
Silica/magnetic GO	195.3	Fang et al., 2020
Silicate-hydrochar composite	214.7	Deng et al., 2020a,b
Silica modified with ethylene diamine	88.9	Kubilay et al., 2007
Salt-based biochars with silicon	152.61	Liu et al., 2020
Fe_2O_3/SiO_2/PAN	113.99	Ramutshatsha et al., 2019
$SiO_2/CuFe_2O_4$/PANI	285.71	this study

properties, and ordered porous structure. The efficiency of the synthesized novel $SiO_2/CuFe_2O_4$/PANI was also found to be high (Table 3). Therefore, the developed composite is a promising scavenger for the selected ions from the synthetic/-contaminated water.

4. Conclusion

SiO_2, $CuFe_2O_4$, and PANI were prepared as starting materials and intercalated to fabricate a new multifunctional ($SiO_2/CuFe_2O_4$/PANI) composite. The developed composite was characterized by different techniques and tested as a new adsorbent for the uptake of Fe(II), Mn(II), and Cu(II) ions in batch mode. The variation of $SiO_2/CuFe_2O_4$/PANI active sites resulted in enhanced removal efficiency compared to single component. The isotherm results indicated that the Fe(II) and Mn(II) interaction with $SiO_2/CuFe_2O_4$/PANI were better fitted to the Langmuir model. The Freundlich equation was most suitable for modelling Cu(II) adsorption. The kinetics study revealed the applicability of the pseudo-first-order model for the scavenging of Fe(II), Mn(II), and Cu(II) from aquatic systems. The adsorption mechanisms were controlled by chelation and electrostatic attractions. This study clearly indicates that the $SiO_2/CuFe_2O_4$/PANI composite can be applied as an effective adsorbent towards heavy metal ions from contaminated waters and wastewaters. Further studies could study the selectivity and scavenging mechanism of the studied ions in multi-adsorption systems including heavy metal ions and organic dyes.

Acknowledgements

The authors would like to thank the Deanship of Scientific Research at Umm Al- Qura University, Saudi Arabia, for supporting this work by Grant Code. 19-SCI-1-01-0033.

Appendix A. Supplementary data

Supplementary data to this article can be found online at https://doi.org/10.1016/j.arabjc.2020.08.028.

References

Awual, M.R., Eldesoky, G.E., Yaita, T., Naushad, M., Shiwaku, H., Alothman, Z.A., Suzuki, S., 2015. Schiff based ligand containing nano-composite adsorbent for optical copper(II) ions removal from aqueous solutions. Chem. Eng. J. 279, 639–647.

Almoisheer, N., Alseroury, F.A., Kumar, R., Almeelbi, T., Barakat, M.A., 2019. Synthesis of graphene oxide/silica/carbon nanotubes composite for removal of dyes from wastewater. Earth Syst. Environ. 3, 651–659.

Aziz, H.A., Tajarudin, H.A., Wei, T.H.L., Alazaiza, M.Y.D., 2020. Iron and manganese removal from groundwater using limestone filter with iron-oxidized bacteria. Int. J. Sci. Environ. Technol., 1–14

Barakat, M.A., Kumar, R., Balkhyoura, M., Taleb, M.A., 2019. Novel Al_2O_3/GO/halloysite nanotube composite for sequestration of anionic and cationic dyes. RSC Adv. 9, 13916.

Barik, B., Kumar, A., Nayak, P.S., Achary, L.S.K., Rout, L., Dash, P., 2020. Ionic liquid assisted mesoporous silica-graphene oxide nanocomposite synthesis and its application for removal of heavy metal ions from water. Mater. Chem. Phys. 239, 122028.

Cabuk, M., Alan, Y., Yavuz, M., Unal, H.I., 2014. Synthesis, characterization and antimicrobial activity of biodegradable conducting polypyrrole-graftchitosan copolymer. Appl. Sur. Sci. 318, 168–217.

Cai, C., Wang, R., Liu, S., Yan, X., Zhang, L., Wang, M., Tong, Q., Jiao, T., 2020. Synthesis of self-assembled phytic acid-MXene nanocomposites via a facile hydrothermal approach with elevated dye adsorption capacities. Colloid. Surface. A. 589, 124468.

Chen, R.P., Zhang, Y.L., Shen, L.F., Wang, X.Y., Chen, J.Q., Ma, A. J., Jiang, W.M., 2015. Lead(II) and methylene blue removal using a fully biodegradable hydrogel based on starch immobilized humic acid. Chem. Eng. J. 268, 348–355.

Da'na, E., Sayari, A., 2013. Modeling adsorption of copper on amine-functionalized SBA-15: predicting breakthrough curves. J. Environ Eng, 2013.

Daka, J.J., Munyati, O.M., Nyirenda, J., 2020. Iron chlorophyll-a as biomimic catalyst for the green synthesis of polyaniline nanostructures: Evaluation, characterization and optimization. Sustain. Chem. Pharm. 15, 100194.

Deng, X., Chen, Y., Wen, J., Xu, Y., Zhu, J., 2020a. Bian Z. Polyaniline-TiO_2 composite photocatalysts for light-driven hexavalent chromium ions reduction. Science Bulletin. 65 (2), 105–112.

Deng, J., Li, X., Wei, X., Liu, Y., Liang, J., Song, B., Shao, Y., Huang, W., 2020b. Hybrid silicate-hydrochar composite for highly efficient removal of heavy metal and antibiotics: coadsorption and mechanism. Chem. Eng. J. 11, 124097.

Dinari, M., Neamati, S., 2020. Surface modified layered double hydroxide/polyaniline nanocomposites: synthesis, characterization and Pb^{2+} removal. Colloid. Surface. A: Physicochem. Eng. Asp. 124438.

Dou, X., Wang, G.C., Zhu, M., Liu, F., Li, W., Mohan, D., 2018. Pittman Jr CU. Identification of Fe and Zr oxide phases in an iron-zirconium binary oxide and arsenate complexes adsorbed onto their surfaces. J. Hazard. Mater. 353, 340–347.

Du, X., Liu, G., Qu, F., Li, K., Shao, S., Li, G., Liang, H., 2017. Removal of iron, manganese and ammonia from groundwater using a PAC-MBR system: the anti-pollution ability, microbial population and membrane fouling. Desalination. 403, 97–106.

Fang, P., Xia, W., Zhou, Y., Ai, Z., Yin, W., Xia, M., Yu, J., Chi, R. A., Yue, Q., 2020. Ion-imprinted mesoporous silica/magnetic graphene oxide composites functionalized with Schiff-base for selective Cu(II) capture and simultaneously being transformed as a robust heterogeneous catalyst. Chem. Eng. J. 385, 123847.

Feng, Y., Yin, J., Liu, S., Wang, Y., Li, B., Jiao, T., 2020. Facile synthesis of Ag/Pd nanoparticle-loaded poly (ethylene imine) composite hydrogels with highly efficient catalytic reduction of 4–nitrophenol. ACS. Omega. 5, 3725–3733.

Fotukian, S.M., Barati, A., Soleymani, M., Alizadeh, A.M., 2020. Solvothermal synthesis of $CuFe_2O_4$ and Fe_3O_4 nanoparticles with high heating efficiency for magnetic hyperthermia application. J. Alloy. Compd. 816, 152548.

Ge, L., Zhang, M., Wang, R., Li, N., Zhang, L., Liu, S., Jiao, T., 2020. Fabrication of CS/GA/RGO/Pd composite hydrogels for highly efficient catalytic reduction of organic pollutants. RSC Adv. 10, 15091–15097.

Gupta, G.S., Yadav, G., Tiwari, S., 2020. Bioremediation of heavy metals: A new approach to sustainable agriculture. In: restoration of wetland ecosystem: A Trajectory Towards a Sustainable Environment. Springer, Singapore, pp. 195–226.

Ho, Y.S., McKay, G., 1999. Pseudo-second order model for sorption processes. Process Biochem. 34 (5), 451–465.

Huang, Z., Zhao, M., Wang, C., Wang, S., Dai, L., Zhang, L., Xu, L., 2020. Selective removal mechanism of the novel Zr-based metal organic framework adsorbents for gold ions from aqueous solutions. Chem. Eng. J. 384, 1233432.

Hussain, M.I., Xia, M., Akhta, R.K., Nawaz, A., Sharma, S.K., Javed, Y., 2020. Ferrite nanoparticles for biomedical applications. In: Magnetic Nanoheterostructures. Springer, Cham, pp. 243–265.

Irshad, S., Xie, Z., Wang, J., Nawaz, A., Luo, Y., Wang, Y., Mehmood, S., 2020. Indigenous strain Bacillus XZM assisted phytoremediation and detoxification of arsenic in Vallisneria denseserrulata. J. Hazard. Mater. 381, 120903.

Jin, Y., O'Connor, D., Ok, Y.S., Tsang, D.C., Liu, A., Hou, D., 2019. Assessment of sources of heavy metals in soil and dust at children's playgrounds in Beijing using GIS and multivariate statistical analysis. Environ. Int. 124, 320–328.

Kumar, R., Kumar, M., Ahmad, R., Barakat, M.A., 2013. L-Methionine modified Dowex50 ion-exchanger of reduced size for the separation and removal of Cu(II) and Ni(II) from aqueous solution. Chem. Eng. J. 218, 32–38.

Kumar, R., Laskar, M.A., Hewaidy, I.F., Barakat, M.A., 2019. Modified adsorbents for removal of heavy metals from aqueous environment: A review. Earth Syst. and Environ. 3, 83–93.

Kubilay, S., Gürkan, R., Şavran, A., Sahan, T., 2007. Removal of Cu (II), Zn(II) and Co(II) ions from aqueous solutions by adsorption onto natural bentonite. Adsorption. 13, 41–51.

Lai, P., Daear, W., Löbenberg, R., Prenne, R.E.J., 2014. Overview of the preparation of organic polymeric nanoparticles for drug delivery based on gelatine, chitosan, poly (D), L-lactide-co glycolic acid) and polyalkylcyanoacrylate. Colloid. Surface. B: Biointerfaces. 118, 154–163.

Liu, J., Cheng, W., Yang, X., Bao, Y., 2020. Modification of biochar with silicon by one-step sintering and understanding of adsorption mechanism on copper ions. Sci. Total Environ. 704, 135252.

Malik, D.S., Jain, C.K., Yadav, A.K., 2017. Removal of heavy metals from emerging cellulosic low-cost adsorbents: a review. Appl. Water Sci. 7, 2113–2136.

Mobasherpour, I., Salahi, E., Pazouki, M., 2012. Comparative of the removal of Pb^{2+}, Cd^{2+} and Ni^{2+} by nano crystallite hydroxyapatite from aqueoussolutions: Adsorption isotherm study. Arab. J chem. 5, 439–446.

Mohammadi, R., Azadmehr, A., Maghsoudi, A., 2019. Fabrication of the alginate-combusted coal gangue composite for simultaneous and effective adsorption of Zn(II) and Mn(II). J. Environ. Chem. Eng. 7, 103494.

Moreno, P.J.C., Garcia-Cuello, V.S., Giraldo, L., 2011. The removal and kinetic study of Mn, Fe, Ni and Cu ions from solutions onto activated carbon from coconut shells. Adsorption. 17, 505–514.

Mujasambatoo, K., Kumar, S., Ansari, M.S., 2011. Ferrimagnetic ordering of Ti^{4+} doped $Mn_{1+x}Fe_{2-2x}O_4$ ($0 \leq x \leq 0.5$) ferrites at room temperature. Sci. Adv. Mater. 3, 120–126.

Ngah, W.S., Ab Ghani, S., Kamari, A., 2005. Adsorption behaviour of Fe(II) and Fe(III) ions in aqueous solution on chitosan and cross-linked chitosan beads. Bioresour. Technol. 96, 443–450.

Ordinartsev, D.P., Sviridov, A.V., Sviridov, V.V., 2018. Extracting vanadium, molybdenum, and tungsten from acidic solutions via adsorption on modified montmorillonite. Russ. J. Phys. Chem. A. 92, 2060–2064.

Ouyang, D., Zhuo, Y., Hu, L., Zeng, O., Hu, Y., He, Z., 2019. Research on the adsorption behavior of heavy metal Ions by porous material prepared with silicate tailings. Minerals. 9, 291.

Patil, D.S., Chavan, S.M., Oubagaranadin, J.U.K., 2016. A review of technologies for manganese removal from solutionss. J. Environ. Chem. Eng. 4, 468–487.

Ramutshatsha, M.D., Ngila, J.C., Ndungu, P.G., Nomngongo, P.N., 2019. Ultrasound assisted adsorptive removal of Cr, Cu, Al, Ba, Zn, Ni, Mn, Co and Ti from seawater using Fe_2O_3-SiO_2-PAN nanocomposite: Equilibrium Kinetics. J. Mar. Sci. Eng. 7, 133.

Reiad, N.A., Salam, O.E.A., Abadir, E.F., Harraz, F.A., 2012. Adsorptive removal of iron and manganese ions from aqueous solutions with microporous chitosan/polyethylene glycol blend membrane. J. Environ. Sci. 24, 1425–1432.

Renu, Agarwal, M., Singh, K., 2017. Heavy metal removal from solutions using various adsorbents: a review. J. Water Reuse Desal. 07, 387–419.

Seliem, M.K., Komarneni, S., 2016. Equilibrium and kinetic studies for adsorption of iron from aqueous solution by synthetic Na-A zeolites: Statistical modeling and optimization. Micropor. Mesopor. Mat. 228, 266–274.

Shao, P., Liang, D., Yang, L., Shi, H., Xiong, Z., Ding, L., Yin, X., Zhang, K., Luo, X., 2020. Evaluating the absorptivity of organo-functionalized silica nanoparticles towards heavy metals: quantitative comparison and mechanistic insight. J. Hazard. Mater. 387, 121676.

Shao, P., Ding, L., Luo, J., Luo, Y., You, D., Zhang, Q., Luo, X., 2019. Lattice-defect-enhanced adsorption of arsenic on zirconia nanospheres: A combined experimental and theoretical study. ACS Appl. Mater. Interfaces. 11, 29736–29745.

Shimano, J.Y., Mac Diarmid, A.G., 2001. Polyaniline, a dynamic block copolymer: key to attaining its intrinsic conductivity. Synth. Met. 123, 251.

Siyal, A.A., Shamsuddin, M.R., Khan, M.I., Rabat, N.E., Zulfiqar, M., Man, Z., Siame, J., Azizli, K.A., 2018. A review on geopolymers as emerging materials for the adsorption of heavy metals and dyes. J. Environ. Manage. 224, 327–339.

Smith, D.W., 1977. Ionic hydration enthalpies. J. Chem. Educ. 54, 540.

Stejskal, J., 2020. Interaction of conducting polymers, polyaniline and polypyrrole, with organic dyes: polymer morphology control, dye adsorption and photocatalytic decomposition. Chem. Papers. 74, 1–54.

Sun, J., Wang, L., Yang, Q., Shen, Y., Zhang, X., 2020. Preparation of copper-cobalt-nickel ferrite/graphene oxide/polyaniline composite and its applications in microwave absorption coating. Prog. Org. Coat. 141, 105552.

Tang, L., Fang, Y., Pang, Y., Zeng, G., Wang, J., Zhou, Y., Deng, Y., Yang, G., Cai, Y., Chen, J., 2014. Synergistic adsorption and reduction of hexavalent chromium using highly uniform polyaniline–magnetic mesoporous silica composite. Chem. Eng. J. 254, 302–312.

Tang, C., Zhang, Y., Han, J., Tian, Z., Chen, L., Chen, J., 2020. Monitoring graphene oxide's efficiency for removing Re(VII) andCr(VI) with fluorescent silica hydrogels. Environ. Pollut. 262, 114246.

Wei, W., Hu, H., Ji, X., Yan, Z., Sun, W., Xie, J., 2018. Selective adsorption of organic dyes by porous hydrophilic silica aerogels from aqueous system. Water Sci. Technol. 78, 402–414.

Yadav, B.V., Gadi, R., Kalra, S., 2019. Clay based nanocomposites for removal of heavy metals from water: A review. J. Environ. Manag. 232, 803–817.

Youssef, A.M., El-Naggar Malhat, M.E., El-Sharkawi, F.M., 2019. Efficient removal of pesticides and heavy metals from solutions and the antimicrobial activity of f-MWCNTs/PVA nanocomposite film. J. Clean. Prod. 206, 315–325.

Yousuf, M.A., Jabeen, S., Shahi, M.N., Khan, M.A., Shakir, I., Warsi, M.F., 2020. Magnetic and electrical properties of yttrium substituted manganese ferrite nanoparticles prepared via micro-emulsion route. Results Phys. 16, 102973.

Zhang, M., Zhu, L., He, C., Xu, X., Duan, Z., Liu, S., Song, M., Song, S., Shi, J., Cao, G., 2019. Adsorption performance and mechanisms of Pb(II), Cd(II), and Mn(II) removal by a β-cyclodextrin derivative. Environ. Sci. Pollut. Res. 26, 5094–5110.

Zhang, W., Sun, A., Zhao, X., Pan, X., Han, Y., Suo, N., Yu, L., Zuo, Z., 2020. Structural and magnetic properties of Ni–Cu–Co ferrites prepared from sol-gel auto combustion method with different complexing agents. J. Alloy. Compd. 816, 152501.

Zhang, Y., Zhao, J., Jiang, Z., Shan, D., Lu, Y., 2014. Biosorption of Fe(II) and Mn(II) ions from aqueous solution by rice husk ash. Biomed. Res, Int, p. 2014.

Zhang, G., Jiuhui Qu, J., Liu, H., a, Adrienne T. Cooper, A.T., Wu, R., 2007. CuFe2O4/activated carbon composite: A novel magnetic adsorbent for the removal of acid orange II and catalytic regeneration, Chemosphere. 68,1058–1068.

Zhao, M., Huang, Z., Wang, S., Zhang, L., 2020. Ultrahigh efficient and selective adsorption of Au(III) from water by novel Chitosan-coated MoS_2 biosorbents: Performance and Mechanisms. Chem. Eng. J. 401, 126006.